LAWRENCE
LIVERMORE
NATIONAL
LABORATORY

LLNL-JRNL-829438

First graded metal Pushered Single Shell capsule implosions on the National Ignition Facility

E. L. Dewald, S. MacLaren, D. Martinez, J. Pino, R. Tipton, D. D. M. Ho, C. Young, C. Horwood, A. R. Vazsonyi, S. Vonhof, G. Mellos, M. Wang, S. Johnson, V. Smalyuk, F. Graziani, E. Monzon, H. Xu, H. Huang, J. Bae, C. Kong, N. Rice

November 22, 2021

Physics of Plasmas

Disclaimer

First graded metal Pushered Single Shell capsule implosions on the National Ignition Facility

E.L. Dewald*, S. MacLaren, D. Martinez, J. Pino, R. Tipton, D.D.-M. Ho, C. Young, C. Horwood, S.F. Khan, E.P. Hartouni, M.S. Rubery, M. Millot, A.R. Vazsonyi, S. Vonhof, G. Mellos, S. Johnson, V.A. Smalyuk, F. Graziani, E. Monzon
Lawrence Livermore National Laboratory, P.O. Box 808, Livermore, CA 94550 USA
H. Xu, H. Huang, J. Bae, C. Kong, N. Rice
General Atomics, San Diego, California 92186, USA
Y.M. Wang
University of California, Los Angeles Samueli School of Engineering, CA 90095 USA
P. Volegov, M.S. Freeman, C. Wilde
Los Alamos National Laboratory, NM 87545 USA

*Graded metal Pushered Single Shell (PSS) capsules are predicted to be a viable alternative to low-Z capsule indirect drive inertial confinement fusion (ICF) implosions for achieving high fusion yields [S.A. MacLaren, et al, Phys. Plasmas **28,** 122710 (2021)]. The first experiments with Be/Cr graded metal PSS capsules indicate that the implementation of the principle design feature, the graded density inner metal layer, has succeeded in producing a stable implosion with performance in agreement with predictions. With 50% Cr concentration in the pusher, PSS capsules have >~2x higher shell densities during stagnation for enhanced core confinement and radiation trapping at ~35% lower shell implosion velocities than low-Z capsules. High energy >30 keV inflight shell radiography recorded 215 km/s implosion velocities and show that implosion Legendre mode P_2 asymmetry can be tuned via inner-to-outer beam wavelength separation, similar to other implosions. Shell radiographs and neutron core images show similar P_2 asymmetry, suggesting no symmetry swings between peak implosion velocity and stagnation times. Despite the modest implosion velocities, gas filled deuterium-tritium capsule implosions generate 10^{15} neutron yields at relatively modest core ion temperatures of 2.75 keV, indicating that in spite of the high density inner layer, the implosions have been stabilized by the design density gradient. When compared to hydrodynamic simulations, the measured yield-over-simulated is 35% due to fuel-pusher mix and other perturbations such as the capsule fill tube. Simple analytical scalings of hot spot pressure and neutron yield show that PSS implosions reach similar performance at lower implosion velocities and higher shell densities to low-Z ICF capsules.*

I. Introduction

In indirect drive experiments on the National ignition Facility[1](NIF), 192 laser beams with up to 2 MJ total energy heat the interior of High-Z hohlraums[2], creating soft x-rays that ablatively compress deuterium-tritium (DT) filled capsules to generate D-T fusion neutron yield. Most of the experiments use low-Z ablators, with a layer close to the fuel being doped with a mid-Z or high-Z material (up to a few percent concentration) to stop M-band or L-band x-rays from the hohlraum preheating the fuel-shell interface[3]. By contrast, Pushered Single Shell (PSS) implosion designs[4,5] employ a high-Z 'pusher' layer at the shell-fuel interface to mitigate core radiation losses. PSS capsules are derived from alternative ignition designs, so-called double shells[6,7] for which the capsule consists of an inner high-Z shell (pusher), containing a gas DT fuel, that traps the core radiation losses (a.k.a. radiation trapping), separated from an outer low-Z ablator shell by a foam layer. PSS capsules combine the double shell pusher and ablator in one single shell that is easier to fabricate without large artifacts. This pusher layer has typically higher density than the ablator and hence the added benefit of enhancing the core tamping which lowers fuel ignition requirements. Generally, the ability of implosions to achieve ignition is characterized by the so-called Lawson parameter $P\tau$ product, where P is the hot spot pressure at stagnation and τ is the burn duration[8,9]. Low-Z capsule implosions aim to achieve high hot spot pressures by increasing the peak implosion velocities at low capsule mass remaining during stagnation. For a total laser drive energy that is similar to low-Z capsule ICF implosions, PSS implosions carry significantly higher pusher peak densities and more capsule mass remaining at stagnation using lower implosion velocities[5,10]. The lower peak implosion velocities also reduce implosion hydrodynamic

*corresponding author dewald3@llnl.gov

instabilities. In simulations the high pusher density allows for similar hot spot pressures as low-Z ICF capsules despite the lower implosion velocity, due to the tamping effect which enhances the core confinement. As a downside for PSS, high-Z material in the pusher can mix with the fuel, compromising ignition.

Previous PSS experiments used a low concentration (~2.5%) Ge dopant as a pusher surrogate at the inner surface of plastic (CH) capsules[11]. Recently, a novel type of PSS capsule was developed that is a blend of mid-Z material (Cr in this case) and Be[5]. The first experiments with these graded metal capsules using gas fuel are summarized in this paper; the experiments were performed on the NIF to tune the capsule implosions for future pusher-fuel mix studies. Section II presents the PSS implosion design and Section III gives a brief description of the various types of experiments. Section IV summarizes the corresponding results and simulations and the paper concludes with a general overall discussion and future directions for further PSS experiments.

II. PSS target and implosion design

Figure 1 shows the PSS capsule pie diagram, Cr concentration and the corresponding density radial profiles, as well as the Cr concentration radial profile as measured versus designed. The gradual increase in dopant concentration was optimized in simulations to increase the robustness of the implosion to Rayleigh Taylor instabilities during the implosion acceleration phase[6]. For the current experiments, the capsule outer radius is 1.14 mm with a full shell thickness of 240 µm. The outer 190 µm consists of a pure Be ablator. A 40 µm wide hyperbolic tangent shaped Cr concentration profile makes the transition from pure Be ablator to ~ 50% Cr, followed by an inner 6 µm wide 50% Cr plateau, forming the pusher. The pusher has a high density of 5 g/cc and provides core tamping and radiation trapping. Finally, the pusher is separated from the gas fuel (50/50 D/T at 6 mg/cc density) by a 2 µm thick pure Be anti-mix layer (Fig. 1b) that, in simulations, prevents the fuel from mixing with the pusher, hence reducing core energy losses.

These Be/Cr capsules are hydrodynamic surrogates for future Be/Mo PSS graded metal capsules; the Be/Cr shells were developed first for implosion tuning experiments due to their lower-Z pusher that is easier to radiograph inflight[12] due to their reduced opacity to backlighting x-rays. Currently under development, the Be/Mo PSS capsules reach 22% Mo in the pusher and will have an identical radial density profiles as the Be/Cr capsules shown in Figure 1b.

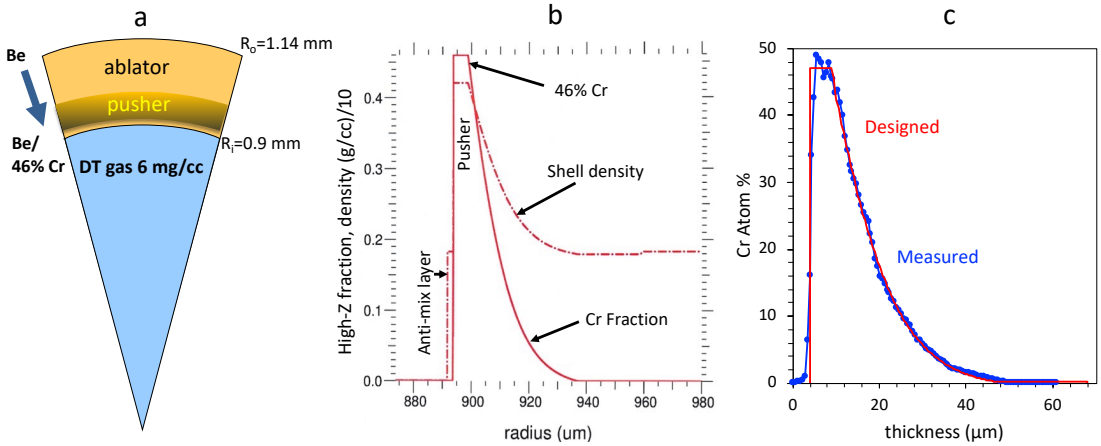

Fig. 1 a) Graded metal PSS capsule pie diagram, b) radial profiles for density (dashed line in units of 10 g/cc) and Cr fraction (solid line) and c) radial profile for Cr concentration as designed (red line) vs measured (blue line).

*corresponding author dewald3@llnl.gov

Following capsule research and development, the first Be/Cr capsules were built for these experiments with a Cr gradient that is close to the design, as shown in Figure 1c. The measured Cr concentration using energy dispersive X-ray spectroscopy (EDS)[13] includes 5 µm spatial blurring, due to the spot size of the excitation electron beam, that is not present in the design profile.

The Be/Cr PSS capsules are centered inside cylindrical Au hohlraums that are 6.72 mm in diameter and 12 mm long, as sketched in Fig. 2a. As is true for most indirect drive experiments on the NIF, the 192 laser beams are distributed in one inner and two outer laser beam rings, and enter the hohlraum through two laser entrance holes (LEHs) that for current experiments are 3.96 mm in diameter.

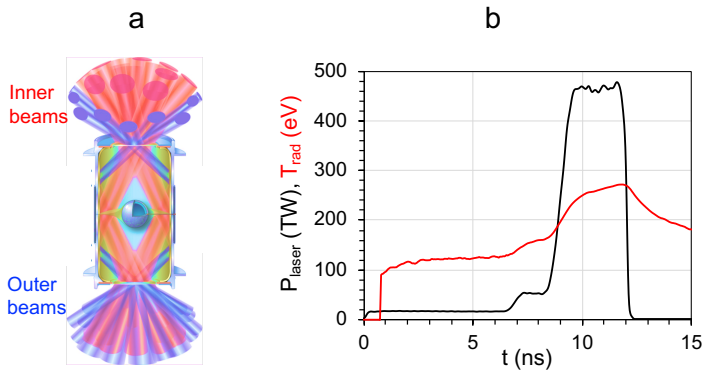

Fig. 2 a) Layout of target and laser beams and b) total laser power (black line) and measured hohlraum radiation temperature (red line).

Complex, high photon energy radiography experiments of the highly opaque PSS capsules were performed at room temperature (293 K), where the hohlraum fill density is limited in order to avoid the LEH windows bursting, as the NIF target chamber is under vacuum. Hence, for all these PSS experiments, the hohlraum is filled with 0.225 mg/cc ^{4}He to tamp the laser heated wall plasma and requires 1 µm thick CH LEH windows to retain the gas fill. This gas fill is lower than for typical ICF hohlraum experiments on the NIF performed at <35 K target temperatures. As shown in Fig. 2b, a 12 ns long 3-shock laser pulse was used with a total peak power of 480 TW and 1.6 MJ energy. Viewing the hohlraum wall at 37.4 deg. from the hohlraum axis through the bottom LEH, the resulting hohlraum soft x-ray drive radiation temperature measured by the Dante broadband spectrometer[14] reaches a peak value of 275 eV at the end of the laser pulse (t=12 ns).

III. Experiments with graded metal PSS capsules

The first experiments with these novel metal-graded capsules were geared towards optimizing shock timing, implosion shape during the implosion and at stagnation, and measuring the capsule implosion velocity. Further, they allow for an initial evaluation of the pusher-fuel mix based on comparisons of the implosion nuclear performance, burn width and hot spot size with simulations. Similar to other implosion types on the NIF, the shock timing both at the capsule equator (facing the hohlraum midplane) and the poles (facing the LEHs) are recorded in a “keyhole” capsule filled with liquid D_2 using the VISAR interferometry diagnostic[15]. These experiments are capable of measuring shock breakout times and shock velocities that are reached during the final rise to peak laser power (t ~ 8.2 ns, Fig. 2b) in D_2, up to ~150 km/s with a ± 5% relative uncertainty.

*corresponding author dewald3@llnl.gov

In low-Z capsule implosions on the NIF, the inflight shell implosion velocity and shape are typically measured in 2D Convergent Ablator (2DConA) backlit radiography experiments, which feature laser heated foils that generate narrow band x-ray sources with photon energies in the 6-16 keV range, depending on the experiment[16]. Due to the high concentration of Cr (Figs. 1b and 1c), the current PSS capsules are opaque to these photon energies. Therefore, following the shock timing experiments, a new setup for inflight capsule radiography was developed that is described in detail in a different study[17] and resembles somewhat the arrangement used for the Compton Radiography of ICF implosions[18]. For radiography, two 25 μm thick Au wires are heated by NIF's Advanced Radiographic Capability (ARC)[19] laser beams with a 1.5 kJ/30 ps laser pulse energy/duration per wire. These wires are placed 30 mm away from the capsule in a 25x magnification point projection arrangement and generate two inflight radiographs separated in time by 0.4 ns. The resulting Au wire bremsstrahlung and Au K-shell emission filtered to >30 keV photon energies are calculated to give a good contrast of the inflight shells at R<~0.3 mm inflight radius when peak implosion velocity is reached[17]. The capsule (Fig. 2a) is radiographed through two 1 mm^2 square shaped cutouts in the hohlraum wall, covered by windows made of 0.1 mm thick high density carbon (i.e., HDC, a.k.a. diamond), that are coated with 4 μm thick Au on the hohlraum interior side to reduce radiation drive losses. Despite the Au coating, the HDC windows are expected to introduce 3D implosion perturbations and cause hohlraum radiation losses when compared to cylindrically symmetric implosions. The radiographs are recorded a time gated hard x-ray detector AXIS (**A**RC **X**-ray **I**maging **S**ystem)[20] that suppresses the hohlraum x-ray background overlap with the radiographs, and on a time integrated image plate (IP)[21] covered with metallic filters. The image plate is placed in front of the AXIS detector, and acts as an additional filter, hence the recorded images are at >30 keV photon energies on the image plate and >50 keV on AXIS. To protect the imager from neutron damage and from neutron induced x-ray background , the capsule D/T (0.5/0.5) gas fuel for these "2DConARC" experiments is replaced with D_2 at the same density of 6 mg/cc; this lowers the neutron yield more than two orders of magnitude due to the lower cross section of the D-D fusion reactions when compared to D-T[22]. The radiographic images provide the shape of the inflight shell at two instances in time, thus also providing the implosion trajectory and an average implosion velocity measurement. Since the PSS capsules provide core radiation trapping, no core emission will escape the capsule that could provide the hot spot shape. Therefore, the core shape is inferred by imaging of the D-D fusion neutrons using the NIF's neutron imager (NIS)[20] that can record a time integrated core image for neutron yields higher than ~1e12 D-D neutrons. By correlating the shape of the inflight shell (R~300 μm) from radiography and that of the core (R~60 μm), we can assess whether the PSS implosions have symmetry swings between the peak implosion velocity and the implosion stagnation times. The line-of-sight of the neutron imager is 191 deg. away in azimuth from the radiography detectors, thus providing core images along nearly the same viewing axis as the radiographs.

Finally, implosions in cylindrically symmetric hohlraums without diagnostic windows (a.k.a. symcaps[24]) were performed using gas D/T (50/50) capsule fill at 6 mg/cc density. They provided accurate information on the nuclear performance of the implosion, stagnation time (a.k.a. bang time BT), implosion burn duration (a.k.a. burn width BW), and first assessment of the pusher-fuel mix effects by comparing the results to hydrodynamic simulations. The NIS diagnostic also provided the core image of D-T fusion neutrons and hence implosion shape at stagnation. While Bang time (BT) information is also provided by 2 MeV D-D neutrons in the 2DConARC experiments, but potential core drift motion introduces a large BT uncertainty compared to that

*corresponding author dewald3@llnl.gov

inferred from 14.1 MeV neutrons generated in the D-T filled symcaps. As a result, the Gamma Reactions History (GRH) diagnostic[25] provides a more precise BT and the first measurement of the implosion burn duration at stagnation.

The experimental data are compared to various hydrodynamic simulations. Integrated hohlraum and capsule 2D simulations were performed with LASNEX[26] including a model for outer-to-inner laser beams cross beam energy transfer (CBET)[27]. For the capsule, the spatial resolution is 1° in the angular direction and has 375 radial zones. For the first mix effects assessment, the data is also compared to 1D LASNEX simulations with 450 zones radial zones using a buoyancy-drag (BD)[28] annular shell-fuel mix model.

The effect of as measured capsule roughness is estimated using high resolution 2D capsule only ARES[29] simulations with and without including a multi-component Navier-Stokes diffusion mix model. For the ARES simulations, the angular resolution is 0.25°, while the radial resolution is 0.5 μm in the Be anti-mix layer and 0.05 μm at the outer ablator[30]. The capsule fill tube, glue spot and supporting tent are not included.

IV. Experimental data and simulations

IV.1 Shock timing experiments

The first shock timing measurements for the metal-graded PSS aimed to measure and adjust the drive shock timing and its pole-to-equator shock timing symmetry such that all shocks merge at the shell-fuel interface, slightly inside the fuel. Figure 3 shows the measured versus simulated laser pulse shape and VISAR data at the capsule pole and waist[15]. For these shock timing experiments, the 2nd shock is delayed by 1 ns and the 3rd shock by 2 ns (Fig. 3a vs Fig. 2b). These changes to the laser pulse allow for precise measurement of the velocities of shocks 1 and 2, as well as the breakout time for shocks 1, and the shock 1-2 and 1-2-3 mergers.

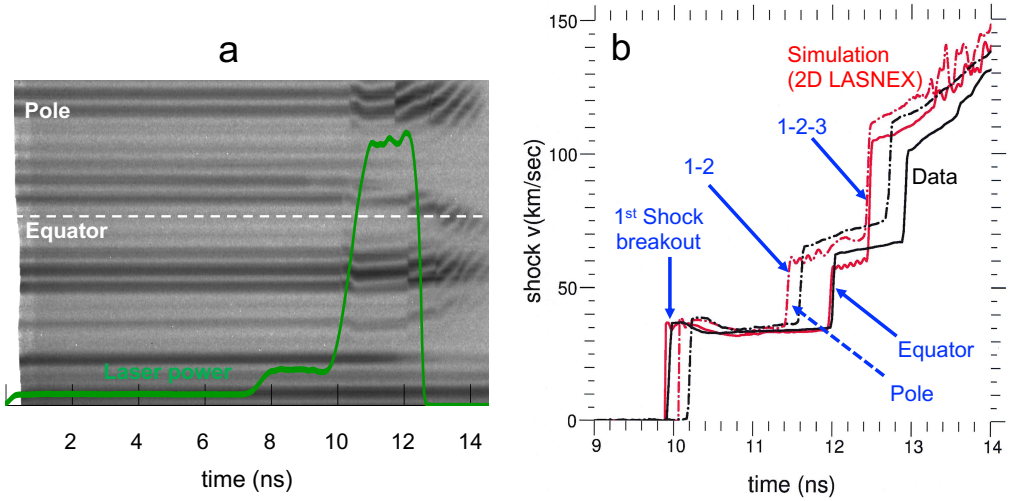

Fig. 3 a) VISAR shock timing data on capsule pole and equator overlapped with the laser power (green line) and b) resulting measured (black lines) and simulated (red lines) shock velocities on capsule pole (dashed lines) and capsule waist (solid lines).

Shock timing data are compared to 2D capsule and hohlraum LASNEX simulations with a CBET model included. This model is tuned to match low-Z Be capsule ICF implosions[31] shock timing

*corresponding author dewald3@llnl.gov

and implosion shape. This is appropriate, since the hohlraum plasma conditions are determined by the laser pulse, Be PSS ablator, hohlraum wall material and gas fill, all of which are similar to these Be capsule ICF implosions. The data and simulations show a reasonable agreement (see Fig. 3b), especially in shock velocities. Discrepancies were observed in the shock 1-2 breakout time in the pole and especially in the shock 1-2-3 breakout time, both at the capsule pole and equator. The discrepancies are attributed to the equation of state (EOS) model used for these Be/Cr capsules which applies Thomas-Fermi scaling of the single Be and Cr components[32]. Currently, work is being done to improve the EOS employed for these capsules. A contributor to the data vs simulation discrepancy in the asymmetry of shock 1-2-3 breakout time may be the time resolved CBET model settings in simulations adjusted previously[31] to match the observed time integrated implosion shape. This is supported by the reasonable agreement in shock breakout symmetry for shocks 1 and 1-2 breakout times when CBET is negligible, based on plasma conditions.

For the capsule implosions following the Keyhole experiments, the breakout times differences between capsule pole and waist observed in the shock timing measurements were minimized by the inner-to-outer beam laser wavelength separation. Until a new EOS model is developed, the data (Fig. 3b) was used directly to adjust the laser pulse (Fig. 2b) in such a way that the 1-2-3 shock merger takes place inside the shell inner surface (shell-fuel interface) at both the capsule waist and poles.

IV.2 Inflight shell radiography experiments

As described in Section III, the implosion velocity and inflight shell shape are measured using point projection radiography in which two high energy (>30 keV) bremsstrahlung x-ray sources were generated by 30 ps long gaussian shaped ARC beams heating 25 μm diameter Au wires[17]. Two snapshots of the D_2 filled inflight capsule, with a delay between the snapshots of 0.4 ns, are recorded on both the AXIS and image plate detectors through hohlraum cutouts covered with Au coated HDC windows. Test experiments preceding the capsule implosions, using an opaque un-driven tungsten carbide (WC) ball with a diameter of 400 μm replacing the capsule, showed that the spatial resolution of the radiographs is similar to the initial Au wire diameter[17]. Time integrated neutron images of the core were recorded to correlate its shape at stagnation (averaged over the burn duration) with the time resolved shape of the inflight shell during peak implosion velocity (inflight shell R in the 200 to 300 μm range) derived from simulations. Figure 4 shows the radiographs of the inflight shell recorded by the AXIS gated imager at photon energies >50 keV and the NIS neutron core images, horizontally flipped to account for the nearly opposite (191°) line of sight difference between the AXIS and the NIS imagers, recorded for two of these experiments.

*corresponding author dewald3@llnl.gov

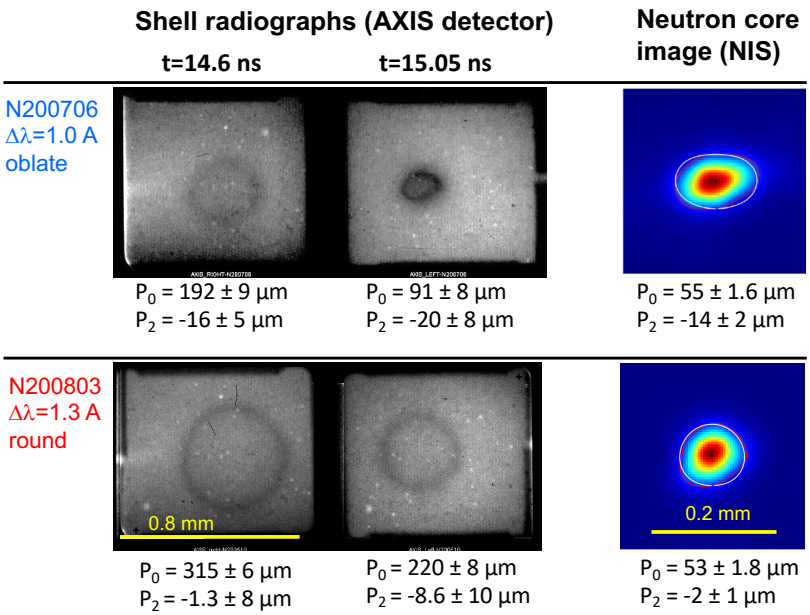

Figure 4 Shell radiographs recorded with the AXIS imager at t=14.6 ns and t=15.05 ns and neutron core images at implosion stagnation (hohlraum axis is vertical) for two experiments: N200706 (first two digits give the shot year, next two the month and the last two the shot day) shows an oblate implosion for an inner-to-outer laser beams wavelength separation of 1A and the following N200803, for which the implosion was tuned round by increasing the wavelength separation to 1.3 A. The inferred capsule P_0 and P_2 coefficients are also shown for all images.

It is important to note that these radiography experiments have a ~5% reduced hohlraum radiation drive as compared to the following symcap implosions during the peak power laser plateau (t> 10 ns, Fig. 2b). The difference is attributed to the drive losses through the HDC windows, overcoated with 4 μm thick Au, due to the fact that the Marshak wave penetration depth in the Au wall exceeds the Au overcoat thickness[3]. For the N200706 and N200803 experiments shown in Fig. 4, the main difference was the increase in the inner-to-outer laser beams wavelength separation from 1 Å on N200706 to 1.3 Å for N200803, applied in the 1 ω (1064 nm) wavelength section of the NIF[1] laser system. The increase in the wavelength separation was intended to reduce the implosion P_2 asymmetry via outer-to-inner cross beam energy transfer (CBET)[27]. It is apparent, however, that the N200706 inflight trajectory is at a smaller inflight capsule radius than for N200803 at the same times. A third experiment labeled N200510, though not included in this paper, showed an implosion trajectory similar to N200803. The reason for a faster implosion trajectory for N200706 is attributed to a ~10% hohlraum x-ray flux increase over N200803 and N200510 as measured by the Dante spectrometer[14]. Since the laser power (Fig. 2b) was very similar between experiments, a possible explanation may be that the hohlraum drive losses in the 4 μm thick Au coating of the HDC windows may vary between experiments, since the coating can have a 25% thickness deviation from nominal. Furthermore, there may be variations in the assembled target gaps between the hohlraum wall cutouts and these Au-coated HDC windows, resulting in hohlraum radiation loss differences between individual targets and thus experiments.

The radius and shape of the inflight shell is analyzed by tracking the x-ray transmission limb minimum in the measured radiographs (Fig. 4). The neutron image core size and shape are analyzed by tracking the 17% contour of peak emission. Figure 5 shows the limb minimum

*corresponding author dewald3@llnl.gov

trajectory measured by AXIS and the IP detectors and the P_2 asymmetry vs P_0 for both the inflight shell and the core.

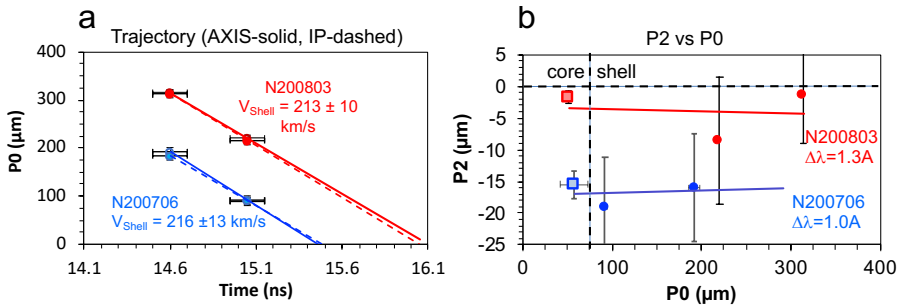

Fig. 5 a) Shell implosion trajectory inferred from limb minimum from AXIS images (solid line fit) and time integrated image plates (IP- dashed line fit); b) – P_2 vs P_0 for the shell measured by AXIS (circles) and core (squares) measured by NIS. All plots are shown for N200706 (in blue) and N200803 (in red) experiments.

As expected, for each experiment, the inferred trajectory is similar between the data recorded by the time resolved AXIS imager and time integrated image plates (Fig. 5a). Despite the fact that N200706 imploded 500 ps earlier (the inflight shell radius is 120 μm smaller), we infer a similar shell average implosion velocity of ~215 km/s for both experiments, which is acceptable given the 15% velocity measurement uncertainty. Furthermore, for N200706 with its late trajectory, the actual peak implosion velocity may be different, possibly larger than for N200803, since the late time data point (P_0<100 μm) is past peak implosion velocity, likely during the deceleration phase. The implosion velocity is ~35% slower than typical ICF implosions with low-Z ablators that have an average implosion velocity 320+/- 50 km/s, which can be explained by the considerably higher shell mass remaining at peak velocity of these novel graded metal PSS capsules.

When we plot P_2 asymmetry vs P_0 (average radius) for the shell and the core, it is evident that they are similar. Furthermore, since the radiographs are recorded earlier than the core measurement at stagnation, both experiments show that there are no P_2 symmetry swings between peak velocity and stagnation times, irrespective of whether P_2 is large, such as for N200706, or small (close to symmetric), such as for N200803.

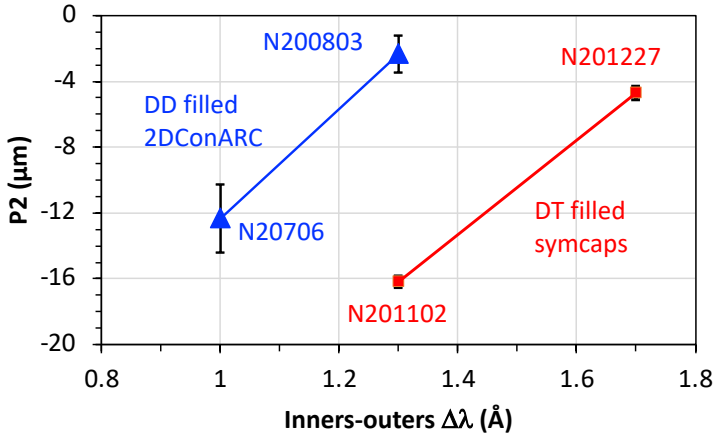

Fig. 6 Core (diamond points) and shell (triangles) P2 asymmetry vs inner-to-outer beams wavelength separation recorded for N200706 (blue points) and N200803 (red points) experiments.

*corresponding author dewald3@llnl.gov

During the first experiment N200706, the observed implosion asymmetry was oblate (i.e., pole hot) with a P_2 of ~-16 μm for an inner-to-outer laser beams wavelength separation of 1 Å . Similar to the shock timing experiments (Section IV.1), 2D LASNEX simulations with CBET[27] included were validated on ICF implosions using Be ablators and similar laser pulses[31]. When these simulations were applied to PSS implosions, they suggested that a wavelength separation increase of 0.3 Å versus N200706 would result in a round implosion. When this wavelength separation increase was applied to N200803, the resulting implosion was indeed nearly round (P_2~-2 μm), despite the hohlraum fill density difference between ICF implosions (0.3 mg/cc ^{4}He fill with 0.5 μm thick LEH window) and PSS implosions (0.225 mg/cc ^{4}He fill with 1 μm thick LEH window). Fig. 6 shows PSS P_2 asymmetry versus laser wavelength separation, which suggests a $\Delta P_2/\Delta\lambda$ sensitivity of 30 ±5 μm/Å inferred from the core P_2 data. Since shell and core P_2 (Figs 4-6) asymmetries are similar, (Fig. 6) we tuned the shape measured via core neutron imaging on the following DT fuel filled symcap implosions.

The nuclear implosion performance was compared to 1D LASNEX calculations using a buoyancy-drag (BD) annular shell-fuel mix model[32] for a first assessment of mix effects, the results of which are summarized in Table 1. For this comparison, we use the N200803 experiment, as the implosion shape is symmetric, giving an appropriate comparison to 1D simulations. The simulated radiation drive is adjusted to match the measured shell trajectory (Fig. 5 LHS).

Table 1: N200803 data vs 1D LASNEX simulations with BD mix included

Parameter	N200803 data	1D LASNEX mix simulations
DD n - yield (e12)	8.7 ± 0.4	11.7
DD T_{ion} (keV)	2.2 ± 0.14	2.40
neutron BT (ns)	15.3 ± 0.3	15.7

In the experiment, the implosion D-D fusion neutron yield, core ion temperature and implosion stagnation time (a.k.a. neutron bang time, or BT) are inferred from 5 neutron time of flight (NToF) diagnostics[33] that record these quantities from various lines of sight, time-integrated over the implosion burn duration. The neutron BT has a much larger uncertainty than other measurement methods used for ICF implosions from core x-ray emission[24], since the time of flight of 2.2 MeV neutrons resulting from D-D fusion reactions[22] is affected by core drift motion and residual kinetic energy of the core at stagnation. The mix simulations summarized here show good agreement with the implosion data when the BD model is initialized with a perturbation amplitude of 160 nm that was chosen to match the measured nuclear yield. The same simulations without mix suggest a yield-over-clean (YoC), defined as the ratio between measured yield and simulated yield without mix, of ~29%; i.e., a 71% nuclear performance degradation due to mix or other perturbations (e.g., from the 10 μm thick fill tube required to fill the capsule with fuel). According to the ARES simulations summarized in the next section, the fill tube and capsule tent perturbations are negligible compared to the mix effects. A better measure of mix effects, including reduced uncertainties in bang time as well as an implosion burn width measurement, was provided by the D-T filled symcap implosions that are summarized in the next section.

IV.3 Implosions with D-T gas filled capsules

*corresponding author dewald3@llnl.gov

The radiographic implosions (Section IV.2) show that the equatorial shape P_2 asymmetry is similar between the inflight shell and the core for both experiments (Figs. 5b and 6). They gave a measure of the implosion trajectory and a first look at the nuclear performance in the presence of 3D implosion shape perturbations inherent for shell radiography. The D-T gas filled symcap implosions summarized in this section are aimed towards evaluating the nuclear performance in the absence of azimuthal shape perturbations and give a first assessment of the shell-fuel mix. While the inflight shape and trajectory cannot be measured, the core shape is inferred from nuclear imaging (NIS), both from the polar and equatorial directions. Furthermore, the implosion stagnation time (a.k.a. neutron bang time) and burn duration are more precisely measured by the GRH diagnostic[25]. For these D-T filled symcap implosions, the laser foot power (t=0-6.5 ns, see Fig. 2) was increased by 10% over the radiography experiments to improve shock timing. Two experiments were executed, the first being N201102 with the same inner-to-outer laser beams wavelength separation of 1.3 Å that resulted in a nearly round implosion for radiography (see N200803 Figs. 4-6). Figure 7 shows the neutron core images recorded for these experiments.

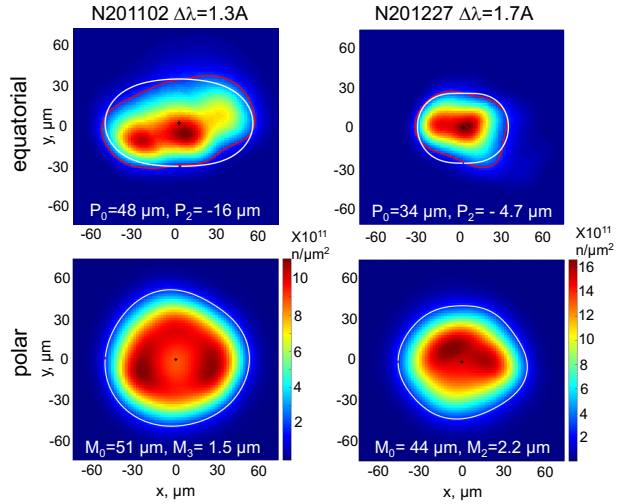

Fig. 7 Equatorial and polar neutron images recorded for experiments N201102 and N201227; the inner-to-outer beams wavelength separation was increased from 1.3 to 1.7 Å, respectively, resulting in a more symmetric implosion, i.e. significant decrease in P_2 asymmetry.

The neutron image for N201102 was oblate, with a P_2=-16 μm. 2D LASNEX simulations without the radiography windows show that this P_2 offset is entirely caused by the 10% increase in the laser power during the foot. Based on the P_2 sensitivity to Δλ measured in radiography (Fig. 6), for the following experiment, N201227, the inner-to-outer laser beams Δλ separation was increased by 0.4 Å (to 1.7 Å), resulting in a core that is nearly round with P_2=-4.7 μm. As shown in Figure 8, core P_2 sensitivity to wavelength separation, $\Delta P_2/\Delta\lambda$ = 30 ±5 μm/Å, is similar for the radiography (Fig. 6) and D-T filled symcaps within measurement uncertainties.

*corresponding author dewald3@llnl.gov

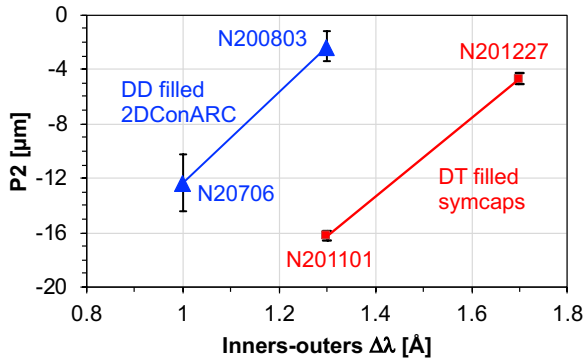

Fig. 8 Core P_2 vs inners-to-outers beams Δλ sensitivity for DD filled capsule 2DConARC (blue triangles and line) and D-T filled symcap (red squares and line) experiments.

The core volume reconstructed using equatorial and polar images (Fig. 7) shows that the volume of N201102 is 2x larger than for N201227. The reduced core compression for N201102 is due to the significant implosion shape P_2 asymmetry.
In addition to neutron imaging, we recorded the nuclear performance of these implosions using the NToF[32] detectors as well as the implosion stagnation time and burn duration using the GRH[25] diagnostics; the results are summarized in Table 2. The table also includes the burn duration (a.k.a. burn width BW) as measured by the GRH diagnostic.

Table 2: Symcap data and 1D LASNEX simulations with BD mix included

Parameter	N201102 data	N201227 data	N201227 1D LASNEX mix sim.
DT n - yield (e15)	0.99 ± 0.03	0.89 ± 0.03	0.965
DT T_{ion} (keV)	2.73 ± 0.1	2.79 ± 0.1	2.83
GRH BT (ns)	15.16 ± 0.03	15.14 ± 0.03	15.15
GRH BW (ps)	237 ± 30	230 ± 30	188
Core P_0, µm	48 ± 0.3	34 ± 0.45	38

The nuclear performance, stagnation time, and burn duration (BW) are similar for both experiments within measurement uncertainties. This is to be expected for gas-filled implosions for which the shape does not have a major effect on the neutron yield degradation. Furthermore, these graded metal capsule implosions recorded among the highest yields of 1e15 D-T fusion neutrons at a relatively modest core ion temperature of ~2.75 keV. The reason for this high neutron yield is the core tamping provided by the high density pusher with 50% mid-Z material concentration.

Compared to the radiography experiments, the symcaps have a stagnation time that is ~0.55 ns earlier due to the missing radiography windows that result in x-ray drive loss at late times. Simulations that match the symcap stagnation time require 10% more drive than those matching measured trajectory in radiography (Fig. 5), which show a 15 km/s higher shell peak implosion velocity in symcaps than the 215 km/s measured in radiography.

The D-T symcap implosions are compared to hydrodynamic simulations that do not account for pusher-fuel mix (i.e., so-called 'clean') and compared to others that account for this mix using the BD mix model[32]. Table 2 compares the nearly round N201227 implosion data to 1D LASNEX BD

*corresponding author dewald3@llnl.gov

mix simulations with a drive multiplier during the peak power to match measured stagnation time which show very good agreement. Clean 1D and 2D LASNEX simulations give a YoC of 35%; i.e., the nuclear yield degradation due to mix is estimated to be 65%. The YoC is only slightly higher than that inferred from radiography experiments (i.e., 29%). This suggests that the implosion 3D shape perturbations' effect due to the radiography windows accounts for ~6% of the degradation on nuclear performance, which is relatively small compared to degradations due to mix or other perturbations, such as those caused by the 10 µm thick capsule fill tube.

We also compare the results with 2D capsule-only hydrodynamic simulations in ARES[29,30]. These simulations include as-built capsule roughness spectrum, but do not include low mode drive asymmetries, capsule fill tube and the associated glue spot or the capsule supporting tent (that holds the capsule inside the hohlraum). Figure 9 shows density and ion temperature maps at stagnation time, with a table comparing simulated and measured implosion performance parameters.

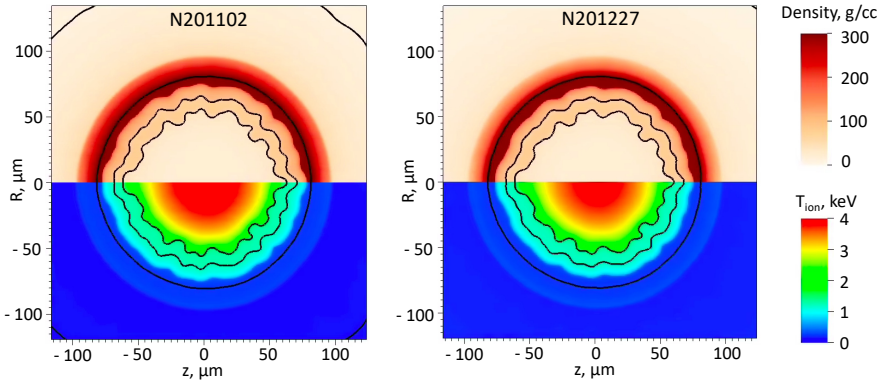

Shot	DT-n yield sim. (exp.)	T_{ion} sim. (exp.) , keV	BT sim. (exp.), ns	BW sim. (exp.), ps
N201102	3.1e15 (0.99 ±.03e15)	2.97 (2.73 ±0.1)	15.16 (15.16 ±0.03)	262 (237 ±30)
N201227	2.33e15 (0.9 ±.03e15)	2.89 (2.79 ±0.1)	15.14 (15.14 ±0.03)	275 (230 ±30)

Figure 9. ARES 2D no mix simulations of the DT filled symcap experiments - top: density and ion temperature maps (hohlraum axis is horizontal) at stagnation and bottom – simulated and measured nuclear performance: neutron yield, ion temperature, stagnation time (i.e. "bang time BT") and burn width (BW).

ARES simulations reach good agreement with the data in all implosion metrics, except for the neutron yield. This is shown by the fact that the data versus simulation deviation is comparable to the data measurement uncertainty. The simulated neutron yield is ~2.6x larger than measured, i.e., YoC is 38% (for N201227, which is fairly symmetric), similar to YoC from 1D LASNEX simulations. ARES simulations including a Multi-Component Navier Stokes (MCNS) diffusive mix model that has previously shown good comparison with deuterated plastic capsules (CD) Mix experiments[11] show a very modest ~2% yield reduction versus clean simulations. This is attributed to the fact that the anti-mix layer placed in the capsule between the pusher and the fuel is efficient in mitigating diffusive mix. The calculations also show that in the absence of low mode asymmetries, the N201102 experiment should have reached ~30% higher neutron yield than N201227 due to a 10% higher density in the pusher at stagnation, whereas in the experiment, similar neutron yields were recorded. One possible explanation for the higher peak density and hence expected yield for N201102 in the absence of low mode asymmetries is a less steep Cr gradient profile for similar capsule roughness (see Fig. 2b,c) than for N201227 leading to lower instabilities and mix. The data versus simulation discrepancy can be explained by the large low

*corresponding author dewald3@llnl.gov

mode implosion asymmetry in the N201102 experiment (Fig. 7) that offsets the higher pusher density effects, resulting in similar neutron yields to N201227.

ARES simulations (Fig. 9) show that while the ion temperatures averaged over both the core volume and burn duration are ~ 2.7 keV as measured by the NToF diagnostics, the peak core temperatures reach 4 keV. Furthermore, very high peak densities of ~300 g/cc are reached in the pusher at stagnation. For this reason, despite the relatively low peak implosion velocities of < 250 km/s as inferred from radiography experiments (Section IV.2), the high pusher densities generate core fuel tamping, resulting in high neutron yields at a modest core temperature and low velocities (Table 2, Fig. 9).

V. Discussion

We compare these first mid-Z graded metal PSS implosions to similar low-Z ablator capsule implosions to estimate the potential differences due to the high density pusher. For a relevant comparison, we choose gas filled fuel experiments of typical low-Z ICF implosions. To quantify the peak shell density (ρ_{max}) effect on implosion performance, we can equate the kinetic pressure of the pusher at peak shell implosion velocity, v_{max}, to the resultant core hot spot pressure at stagnation, $p_{hot\ spot}$, through[34]:

$$p_{hot\ spot}=(n.k.T_{ion})_{hot\_spot} = 4/3\ \rho_{max}.v_{max}^2\ , \qquad [1]$$

where T_{ion} is the hot spot temperature at stagnation, k is the Boltzmann constant and n is the number density of deuterium and tritium atoms in the core. As compared to a low-Z shell implosion, a PSS capsule v_{max} is lower by ~35%, so the v_{max}^2 term in the kinetic pressure is ~2.5x smaller. ARES simulations (Fig. 9) show that PSS peak pusher density reaches 20 g/cc at peak implosion velocity as compared to 300 g/cc at stagnation, the difference being due to the smaller shell radius at stagnation of 60 μm versus 200 μm during peak implosion velocity. Non-igniting low-Z capsule implosions typically reach 5-10 g/cc pusher density at peak implosion velocity and 150 g/cc at stagnation. Thus, at peak implosion velocity, the peak shell density, ρ_{max}, is ~2.5 times larger for PSS than HDC capsules, resulting in a roughly similar kinetic pressure of the shell at peak implosion velocity. Therefore, we estimate that the hot spot pressure is similar between PSS and Low-Z capsule implosions and hence for a similar core fuel density, PSS implosions can reach similar core T_{ion} at stagnation at larger peak pusher densities and lower implosion velocities than low-Z capsules. The implosion neutron yield Y scales as[34]:

$$Y \sim n_D\ n_T\ T_{ion}^4\ \tau_{burn} V_{core}\ , \qquad [2]$$

where τ_{burn} is the burn duration, and V_{core} is the imploded core volume. For Equation (2), we used the D-T reactivity fit $<\sigma v> \sim T_{ion}^4$ which is appropriate for burn averaged T_{ion} in the 2.5 to 4.0 keV range of these experiments[22,34]. While Equation (1) is a kinetic-to-hot-spot pressure balance that is roughly similar for the two implosion types, the ~1.5x larger pusher density at stagnation for PSS enhances core confinement, hence tamping and burn duration compared to low-Z capsules. This can in turn generate more fusion yield for PSS capsules as suggested by recent simulations[5].

Table 3: Comparison of N201227 (PSS implosion) to N200215 (ICF implosion) with HDC capsule

Parameter	N200215 HDC	N201227 PSS

*corresponding author dewald3@llnl.gov

Fill density, mg/cc	4.0	6.0
v_{max}, approx., km/s	340 ± 50	230 ± 50
DT n - yield (e15)	1.18 ± 0.03	0.89 ± 0.03
DT T_{ion} (keV)	3.92 ± 0.1	2.79 ± 0.1
GRH BW (ps)	215 ± 30	230 ± 30
n-yield msrd /expected Eq. (2) norm. to N200215	1	0.9/0.6

We compare N201227 PSS to N200215 - a typical D/T gas fuel implosion using a low-Z high density carbon (HDC a.k.a. diamond)[30] ablator, with the results shown in Table 3. One must note that the HDC capsule implosion used 4.0 mg/cc fuel density, which is 33% lower than for the PSS implosions that reach similar yields at 35% lower implosion velocities and at 40% lower core temperatures. In these first studies, we did not observe an increase in the burn duration outside the GRH measurement errors, which are too large to observe a difference. It should be considered that in simulations, the mix lowers the burn duration; in experiment N201227 for example, BW is lowered by 25% when adding the BD mix model. Thus, more studies will be performed in the future on mix effects versus burn duration.

Furthermore, both HDC and PSS experiments shown in Table 3 have similar YoC values. Per Equation (1), the kinetic pressure for PSS is similar for these implosions at lower implosion velocity and higher pusher density (Fig. 9, Table 3). Since YoC and core radius are similar, we can hypothesize that the fuel mass PSS/HDC ratio is preserved from initial conditions to stagnation for the comparison. For roughly the same kinetic pressure and hence hot spot pressure at stagnation, the 50% higher fuel density for PSS results in proportionally lower T_{ion} for PSS, consistent with the measurements (Table 3). We use Equation (2) to estimate the expected neutron yield for PSS relative to the HDC capsules. For the shown comparison and in the frame of our assumption, the core fuel mass n.V and hence n.V.τ_{burn} is 50% larger for the PSS capsule. Therefore, the neutron yield for PSS relative to HDC capsules should scale roughly as $n^2.T_{ion}^4$ ratio for these experiments. Using this scaling, through their higher fuel density and lower T_{ion}, for PSS we expected a neutron yield that is 1.5x lower than for the HDC capsule, versus the 1.22x measured. Thus, the higher-than-expected neutron yield for the PSS capsule may benefit from enhanced core confinement done by the pusher, despite these initial studies not showing a clearly increased burn duration than for the HDC capsule outside of measurement uncertainties.

VI. Conclusion and future directions

The initial experiments summarized in this paper show that mid-Z/Be graded metal PSS capsules have stabilized the implosion against the dense inner layer through the implementation of a cleverly designed density gradient. This demonstration strengthens the argument presented in Reference 5 that the PSS is a promising alternative to low-Z capsule ICF designs to achieve high fusion yields. The PSS achieves similar nuclear performance to low-Z designs through high pusher mass and peak densities remaining at stagnation, which generate enhanced core tamping at lower implosion velocities when compared to low-Z capsule ICF implosions.

Future experiments will compare PSS implosions using 2-Shock and 3-Shock laser pulses to study the balance between compression and mix that in simulations are both higher for 3-Shock pulses. We will down-select between these laser pulses based on YoC and nuclear performance. Later on,

*corresponding author dewald3@llnl.gov

we will attempt to boost the capsule drive, possibly using alternative hohlraum shapes[34] and study fuel-pusher mix effects as a function of the anti-mix layer (placed between the pusher and the fuel, see Fig. 2) and the fuel density that controls the capsule convergence ratio. We will also compare implosions with mid-Z Cr and high-Z Mo pushers to study the effect of pusher Z on performance and mix.

AKNOWLEDGEMENT
This work performed under the auspices of U.S. Department of Energy by Lawrence Livermore National Laboratory under Contract DE-AC52-07NA27344. This document was prepared as an account of work sponsored by an agency of the United States government. Neither the United States government nor Lawrence Livermore National Security, LLC, nor any of their employees makes any warranty, expressed or implied, or assumes any legal liability or responsibility for the accuracy, completeness, or usefulness of any information, apparatus, product, or process disclosed, or represents that its use would not infringe privately owned rights. Reference herein to any specific commercial product, process, or service by trade name, trademark, manufacturer, or otherwise does not necessarily constitute or imply its endorsement, recommendation, or favoring by the United States government or Lawrence Livermore National Security, LLC. The views and opinions of authors expressed herein do not necessarily state or reflect those of the United States government or Lawrence Livermore National Security, LLC, and shall not be used for advertising or product endorsement purposes.

DATA AVAILABILITY
Raw data were generated at the National Ignition Facility large scale facility. Derived data supporting the findings of this study are available from the corresponding author upon reasonable request.

References
[1]G.H. Miller, E.I. Moses, C.R. Wuest, *Nucl. Fusion* **44,** 228 (2004).
[2]G.D. Tsakiris, J. Massen, R. Sigel, F. Lavarenne, R. Fedosejevs, J. Meyer-ter-Vehn, K. Eidmann, S. Witkowski, H. Nishimura, Y. Kato, H. Takabe, T. Endo, K. Kondo, H. Shiraga, S. Sakabe, T. Jitsuno, M. Takagi, C. Yamanaka, S. Nakai, *Phys. Rev. A* **42**, 6188 (1990); W.A. Stygar, R.E. Olson, R.B. Spielman, R.J. Leeper, *Phys. Rev. E* **64**, 026410 (2001).
[3] J.D. Lindl, P. Amendt, R.L. Berger, S.G. Glendinning, S.H. Glenzer, S.W. Haan, R.L. Kauffman, O.L. Landen, *Phys. Plasmas* **11**, 339 (2004); J. Lindl et al, *Phys. Plasmas* **21**, 020501 (2014).
[4]J. Milovich, P. Amendt, M. Marinak, H.F. Robey, *Phys. Plasmas* **11**, 1552 (2004).
[5]S.A. MacLaren, D.D-M. Ho, O.A. Hurricane, E.L. Dewald, D.A. Martinez, R.E. Tipton, J.E. Pino, C.V. Young, H.W. Xu, C.W. Kong, K. Sequoia, Phys. Plasmas **28,** 122710 (2021).
[6]W.S. Varnum, N.D. Delamater, S.C. Evans, P.L. Gobby, J.E. Moore, J.M. Wallace, R.G. Watt, J.D. Colvin, R. Turner, V. Glebov, J. Soures, C. Stoeckl, *Phys. Rev. Lett.* **84**, 5153 (2000).
[7]D.S. Montgomery, W.S. Daughton, B.J. Albright, A.N. Simakov, D.C. Wilson, E.S. Dodd, R.C. Kirkpatrick, R.G. Watt, M.A. Gunderson, E.N. Loomis, E.C. Merritt, T. Cardenas, P. Amendt, J.L. Milovich, H.F. Robey, R.E. Tipton, M.D. Rosen, *Phys. Plasmas* **25**, 092706 (2018).
[8]J.D. Lawson, "Some criteria for a power producing thermonuclear reactor," *Proceedings of the Physical Society*, Section B **70**, 6–10 (1957).
[9]J. Lindl, S. Haan, O. Landen, A. Christopherson, R. Betti, *Phys. Plasmas* **25**, 122704 (2018).
[10]D.D.-M. Ho, S. A. MacLaren, Y.M. Wang, *APS Division of Plasma Physics, 60th Annual Meeting,* BAPS.2018.DPP.PO6.11 (2018).

*corresponding author dewald3@llnl.gov

[11]E.L. Dewald, J.E. Pino, R.E. Tipton, J.D. Salmonson, J. Ralph, E. Hartouni, S.F. Khan, R. Hatarik, C.V. Young, D. Thorn, V.A. Smalyuk, R. Sacks, A. Nikroo, N. Rice, S.A. MacLaren, S. Prisbrey, B.A. Remington, F. Graziani, *Phys. Plasmas* **26**, 072705 (2019).
[12]E.L. Dewald, S. MacLaren, D. Martinez, R. Tipton, D.D. Ho, et.al., *APS Division of Plasma Physics, 62nd Annual Meeting*, BAPS.2020.DPP.GO11.00010 (2020).
[13]H. Xu, H. Huang, J. Walker, C. Kong, N.G. Rice, M.P. Mauldin, J.D. Vocke, J.H. Bae, W. Sweet, F.H. Elsner, M.P. Farell, C. Alford, T. Cardenas, E. Loomis, *Fusion Sci. Technol.* **73**, pp 354-362 (2018).
[14]E.L. Dewald, K.M. Campbell, R.E. Turner, J.P. Holder, O.L. Landen, S.H. Glenzer, R.L. Kauffman, L.J. Suter, M. Landon, M. Rhodes, and D. Lee, *Rev. Sci. Instrum.* **75**, 3759 (2004).
[15]H.F. Robey, T.R. Boehly, P.M. Celliers, J.H. Eggert, P.M. Celliers, D. Hicks, R.F. Smith, R. Collins, M.W. Bowers, K.G. Krauter et al, *Phys. Plasmas* **19,** 042706 (2012).
[16]J.R. Rygg, O.S. Jones, J.E. Field, M.A. Barrios, L.R. Benedetti, G.W. Collins, D.C. Eder, M.J. Edwards, J.J. Kroll, O.L. Landen *et al*, *Phys. Rev. Lett.* **112**, 195001 (2014).
[17]D. Martinez, E.L. Dewald, S. MacLaren, C. Young, R. Tipton, D.D. Ho, J.E. Pino, D.H. Kalantar, S. Johnson, S. Vonhof, *APS Division of Plasma Physics, 61st Annual Meeting*, BAPS.2019.DPP.JP10.133 (2018)
[18]R. Tommasini, O. L. Landen, L. Berzak Hopkins, S. P. Hatchett, D.H. Kalantar, W. W. Hsing, D.A. Alessi, S.L. Ayers, S.D. Bhandarkar, M.W. Bowers, et al., *Phys. Rev. Lett.* **125**, 155003 (2020).
[19]J.E. Heebner, R.L. Acree Jr., D.A. Alessi, A.I. Barnes, M.W. Bowers, D.F. Browning, T.S. Budge, S. Burns, L.S. Chang, K.S. Christensen, et al., *Appl. Opt.* **58**, 8501 (2019).
[20]G. Hall, N. Izumi, R. Tommasini, A.C. Carpenter, N.E. Palmer, R. Zacharias, B. Felker, J.P. Holder, F.V. Allen, P.M. Bell, D. Bradley, R. Montesanti, O.L. Landen,*Rev. Sci. Instrum.* **85**, 11D624 (2014).
[21]A.L. Meadowcroft, C.D. Bentley, E.N. Stott, *Rev. Sci. Instrum.* **79**, 113102 (2008).
[22]S. Atzeni, J. Meyer-ter-Vehn, *The Physics of Inertial Confinement Fusion*, p. 20, Oxford University Press (2004).
[23] P. Volegov, C. R. Danly, D. N. Fittinghoff, G. P. Grim, N. Guler, N. Izumi, T. Ma, F.E. Merrill, A.L. Warrick, C.H. Wilde, and D.C. Wilson, Rev. Sci. Instrum. 85, 023508 (2014).
[24]O.L. Landen, T.R. Boehly, D.K. Bradley, D.G. Braun, D.A. Callahan, P.M. Celliers, G.W. Collins, E.L. Dewald, L. Divol, S.H. Glenzer, A. Hamza, D.G. Hicks, N. Hoffman, N. Izumi, O.S. Jones, R.K. Kirkwood, G.A. Kyrala, P. Michel, J. Milovich, D.H. Munro, A. Nikroo, R.E. Olson, H.F. Robey, B.K. Spears, C.A. Thomas, S.V. Weber, D.C. Wilson, M.M. Marinak, L.J. Suter, B.A. Hammel, D.D. Meyerhofer, J. Atherton, J. Edwards, S.W. Haan, J.D. Lindl, B.J. MacGowan, E. I. Moses, *Phys. Plasmas* **17**, 056301 (2010).
[25] H.W. Herrmann, N. Hoffman, D.C. Wilson, W. Stoeffl, L. Dauffy, Y.H. Kim, A. McEvoy, C.S. Young, J.M. Mack, C.J. Horsfield, M. Rubery, E.K. Miller, Z.A. Ali, *Rev. Sci. Instrum.* **81** , 10D333 (2010).
[26] J. Nuckolls, L. Wood, A. Thiessen, and G. B. Zimmerman, *Nature*, **239**, 5368, pp. 139–142 (1972)
[27] P. Michel, L. Divol, E. A. Williams, S. Weber, C.A. Thomas, D. A. Callahan, S.W. Haan, J. D. Salmonson, S. Dixit,D. E. Hinkel, M. J. Edwards, B. J. MacGowan, J. D. Lindl, S. H. Glenzer, and L. J. Suter, *Phys. Rev. Lett.* **102**, 025004 (2009).
[28]Y. Zhou, G.B. Zimmerman, E.W. Burke, *Physical Rev. E* **65**, 056303 (2002).
[29]R.M. Darlington, T.L. McAbee, G. Rodrigue, *Comput. Phys. Commun.* **135**, 58 (2001).

*corresponding author dewald3@llnl.gov

[30]K. Mackay and J. Pino, *Phys. Plasmas* **27**, 092704 (2020)
[31]A.B. Zylstra, S. MacLaren, S.A. Yi, J. Kline, D. Callahan, O. Hurricane, B. Bachmann, G. Kyrala, L. Masse, P. Patel, J.E. Ralph, J. Salmonson, P. Volegov, C. Wilde, *Phys. Plasmas* **26**, 052707 (2019).
[32]R.M. More, K.H. Warren, D.A. Young, G.B. Zimmerman, *Phys. Fluids* **31**, 3059 (1988); D.A. Young, E. Corey, *J. Appl. Phys.* **78**, 3748 (1995).
[33]R. Hatarik, R.C. Nora, B.K. Spears, M.J. Eckart, G.P. Grim, E.P. Hartouni, A.S. Moore, D.J. Schlossberg, Rev. Sci. Instrum. 89, 10I138 (2018).
[34]E.L. Dewald, R. Tommasini, N.B. Meezan, O.L. Landen, S. Khan, R. Rygg, J. Field, D. Sayre, A.J. MacKinnon, L.F. Berzak Hopkins, S. Le Pape, A. Pak, C.A. Thomas, M. Farell, A. Nikroo, O. Hurricane, *Phys. Plasmas* **25**, 092702 (2018).
[35]A. Casner, T. Jalinaud, L. Masse, D. Galmiche, *Phys. Plasmas* **25**, 092702 (2018).

*corresponding author dewald3@llnl.gov